A crystallization and structural study of the compound $Pb_2V_2O_7$ synthesized by a facile sol–gel-based chemical route

A. Suárez-Gómez, Santiago J. A. Figueroa, Diego G. Lamas & Julio C. Cezar

Journal of Sol-Gel Science and Technology

ISSN 0928-0707

J Sol-Gel Sci Technol
DOI 10.1007/s10971-015-3698-0

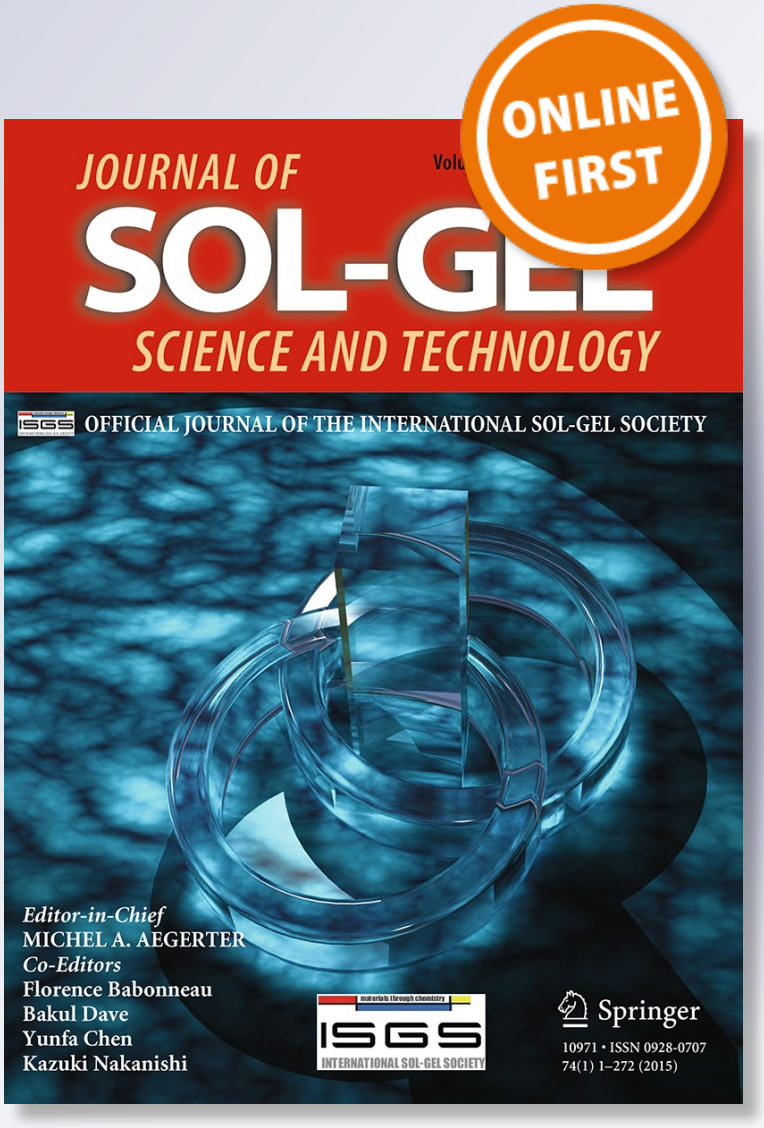

Springer

J Sol-Gel Sci Technol
DOI 10.1007/s10971-015-3698-0

ORIGINAL PAPER

A crystallization and structural study of the compound $Pb_2V_2O_7$ synthesized by a facile sol–gel-based chemical route

A. Suárez-Gómez[1] · Santiago J. A. Figueroa[2] · Diego G. Lamas[3] · Julio C. Cezar[2]

Received: 10 November 2014 / Accepted: 29 March 2015

Abstract In this work, we carried out the synthesis of lead(II) divanadate(V) by means of a soft chemistry reaction based on a sol–gel-derived route. The final organic precursor was heat treated ($T = 400$, 500, 600, 750 and 800 °C) and structurally analyzed for each temperature by taking into account the results of FTIR spectroscopy, synchrotron X-ray powder diffraction and X-ray absorption near-edge structure. As an overall result, we report a final compound with remarkable crystallographic and morphological qualities that seem to keep all its structural features in the temperature range 450–700 °C before the structure incongruently melts. As a highlight, the desired material was obtained following a highly reproducible, low-cost, low-temperature and quite straightforward chemical route. Besides, this synthesis route could also allow the appropriate integration of lead(II) divanadate(V) nanoparticles, or nanolayers, into more complex systems as well as the feasibility for being expanded to other materials.

Electronic supplementary material The online version of this article (doi:10.1007/s10971-015-3698-0) contains supplementary material, which is available to authorized users.

✉ A. Suárez-Gómez
amaury.sg@gmail.com

[1] Universidad de Guadalajara, Centro Universitario de Los Valles, Carr. Guadalajara-Ameca km 45.5, CP 46600 Ameca, JAL, Mexico

[2] Brazilian Synchrotron Light Laboratory (LNLS)/Brazilian Center of Energy and Materials (CNPEM), CP 6192, Campinas, SP 13083-970, Brazil

[3] CONICET - Escuela de Ciencia y Tecnología, Universidad Nacional de Gral. San Martín, San Martín, Pcia. de Buenos Aires, Argentina

Published online: 08 April 2015

Graphical Abstract

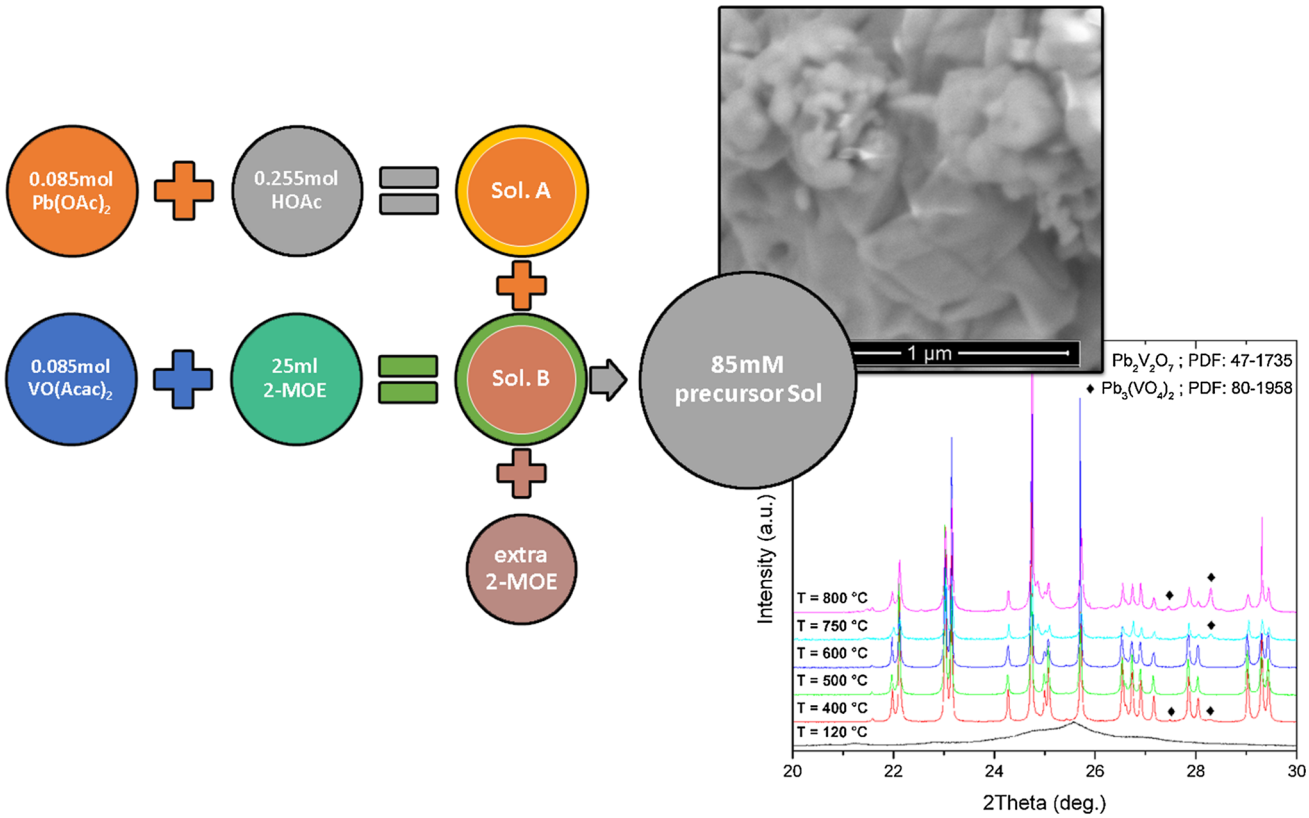

Keywords Divanadates · Synchrotron · $Pb_2V_2O_7$ · Sol–gel · Nanoparticles

1 Introduction

Orthovanadates(V) and divanadates(V) of divalent metals are well-known catalytic agents for the synthesis of several organic compounds and are currently receiving special attention due to their potential application in sensors and photocatalysts, among other fields [1, 2]. Particularly, lead(II) divanadate(V), $Pb_2V_2O_7$, has the potential for being used as a precursor for the synthesis of the relatively new multiferroic perovskite $PbVO_3$ [3, 4] and the magnetic $Pb_2FeV_3O_{11}$ [5, 6] or for the flux growth synthesis of laser-host orthovanadate systems [7, 8]. This material has been mostly synthesized by usually following a powder-based solid-state reaction using the corresponding oxides as precursors and treating the fired powders according to certain thermal regimes [9, 10]. This procedure, depending on the temperature values that are reached, sometimes demands a rigorous atmosphere control to avoid the volatility of several species, mostly lead, that tend to volatilize as PbO around 850 °C; see, for instance, a typical flux growth procedure as described in [8]. Chemical route synthesis for this compound, on the other hand, are not common and, among them, it must be highlighted the composite-hydroxide-mediated (CHM) procedure that was practically universalized in [11].

In this work, we will show the chemical synthesis of $Pb_2V_2O_7$ by means of a facile three-step sol–gel-based route at room conditions, without any special requirement or dedicated care and very cost-effective. We will also try to elucidate the best crystallization conditions as well as further transformations that the material could be able to experiment according to the treatment environment and composition. Some structural features will also be discussed. Our experimental route has been described on previous works for a different system [12], and this study is also an attempt to expand the method into other relevant materials.

2 Materials and methods

2.1 Synthesis

Our starting reagents were lead(II) acetate trihydrate ($Pb(OAc)_2{\cdot}3H_2O$, Aldrich, 99.99 % pure), acetic acid (HOAc, Aldrich, 99.7 %), vanadyl acetylacetonate ($VO(Acac)_2$, Aldrich, 98 %) and 2-methoxyethanol anhydrous (2-MOE, Aldrich, 99.8 %), which reacted according to the flow diagram depicted in Fig. 1.

Fig. 1 Schematic of the sol–gel-based route used in this work

As it was mentioned above, the proposed route follows a similar, although simpler, approach as the three-step method that we have described elsewhere [13]. As can be seen, lead acetate is dissolved in acetic acid with a 1:3 molar ratio at 120 °C during 3 h, forming a solution that we will call Sol. A. At the same time, the appropriate amount of the vanadyl compound is dissolved in 2-MOE slightly above room temperature (~33 °C) until a complete dissolution, referred as Sol. B, is verified. In this step, the amount of 2-MOE could be freely chosen by the researcher by taking into account the desired final concentration. Afterward, both solutions were mixed in the presence of some extra 2-MOE that, if needed, helps to rectify and/or fix the final precursor solution, and this final solution was kept stirring at room temperature for about 10–12 h. for homogenizing and stabilizing purposes. Even though we carried out several successful syntheses for concentrations ranging from 8.5 mM to 350 mM, the flow diagram shown in Fig. 1 depicts the synthesis of a typical 85 mM precursor sol which, without any particular reason, was the precursor chosen for this study.

In the final step, our solution was dried at 120 °C and heat treated at 400, 500, 600, 750 and 800 °C as the structure was inspected for each of these temperatures. The environment, in every step of the synthesis procedure, was simply the room condition, and treatments were performed in air.

2.2 Experimental techniques

In order to explore the structure and morphology of the treated materials, samples were characterized by means of Fourier transform infrared spectroscopy (FTIR) performed in transmission mode in an FTIR660 spectrophotometer, X-ray diffraction (XRD) and X-ray absorption near-edge structure region (XANES), with both experiments being performed at the LNLS facility in Campinas, Brazil.

The X-ray powder diffraction experiments were carried out using the synchrotron D10B-XPD beamline. A high-resolution configuration with a Ge (1 1 1) crystal analyzer was used at a working wavelength of 1.3761 Å. On the other hand, the average crystallite size of all the samples was determined by means of the Scherrer equation using a Si standard (NIST SRM 640d) to subtract the instrumental broadening and considering a Scherrer constant of 0.94 while describing the peak width with the corresponding full width at half maximum (FWHM) parameter.

In the case of the XANES experiment, the synchrotron D04B-XAFS1 beam line was used. In this experiment, the vanadium K-edge spectra were collected in transmission mode using a Si (1 1 1) single channel-cut crystal monochromator at room conditions with a slit aperture of 0.5 mM, to obtain an energy resolution of about 1 eV [14]. The three ion chambers as detectors were filled with N_2 and He in the right proportion in order to have an absorption of 10 % in I_0 and 70 % in I_1. The energy calibration was obtained by simultaneous absorption measurements on the vanadium metal sample positioned between the second and the third ionization chambers.

Further experimental or processing details will be given, if required, in the Sect. 3 of this work.

3 Results and discussion

3.1 X-ray diffraction

Figure 2 shows the XRD experimental patterns recorded for our samples. These diffraction data were found to be in a very good agreement with a previously reported powder

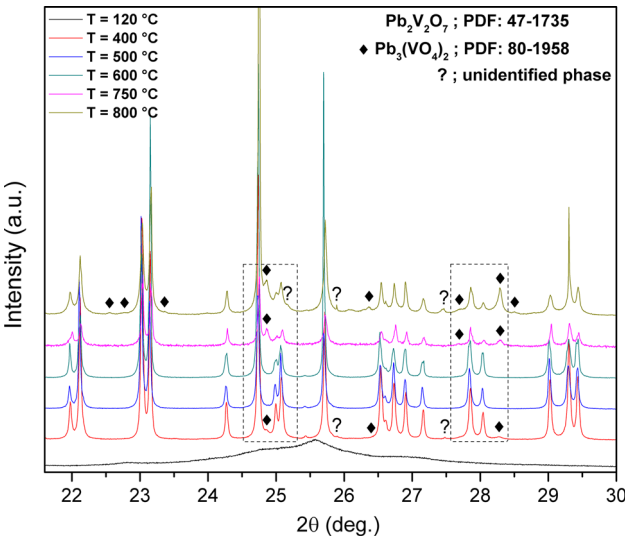

Fig. 2 Recorded XRD patterns for the $Pb_2V_2O_7$ precursors treated at different temperatures. Detected and identified phases, as well as an unidentified one, are highlighted and referenced whenever present. *Dotted* regions appear expanded in Fig. 3

diffraction file (PDF) included in the International Centre for Diffraction Data (ICDD) PDF-2 database for the $Pb_2V_2O_7$ compound, and consequently, the corresponding reference number is shown in the graph.

As was expected for our synthesis procedure, an amorphous precursor usually rich in acetate and methoxyethoxy complexes turns into a polycrystalline material when treated at the appropriate temperatures [15]. In this case, the material seems to crystalize very well when fired beyond 400 °C. At this temperature, it was detected the coexistence of two minority secondary phases that are highlighted with symbols (filled diamond and ?) in Fig. 2. The identified phase (filled diamond) of these two corresponds to the $Pb_3(VO_4)_2$ compound with space group $P2_1/c$, an expected intermediate and stable phase that could be present right before a complete crystallization is attained. On the other hand, the second one (?) could not be univocally identified given its poor contribution to the diffractograms recorded in our experiments but, to no surprise, can be associated with any of the numerous defective non-stoichiometric lead vanadate compounds that, as has been reported, commonly arise and stabilize in the vicinity of the single-phase treatment conditions [16–18].

Dotted regions in Fig. 2 are shown as expanded graphs in Fig. 3a, b along with nonlinear least square fittings (NLLSF) based on pseudo-Voigt line profile shapes that were carried out in order to determine the lattice parameters of the predominant phase—$Pb_2V_2O_7$; space group $P2_1/a$—for each temperature. These profile lines were indexed according to the ICDD-PDF files shown in Fig. 2 and their temperature evolution can also be clearly seen on the expanded graphs.

As a result, Table 1 shows the lattice parameters determined from the profile peak fitting described above along with the average crystallite size ($<D_C>$) that, as can be seen, suffered just slight variations in the whole temperature range under analysis.

According to these results, and taking into account the small amount of the secondary phase at 400 °C, an optimal crystallization temperature in our case should be similar to the 430 °C reported in [9], with further treatments around 600 °C in that report, and undoubtedly well below the 700–800 °C regime described in 3, something that in our experiments brought undesired results that are, by the way, in good correspondence with the already-reported incongruent melting for this system at 740 °C [18]. At $T = 750$ °C, as shown in Fig. 3, diffraction patterns clearly

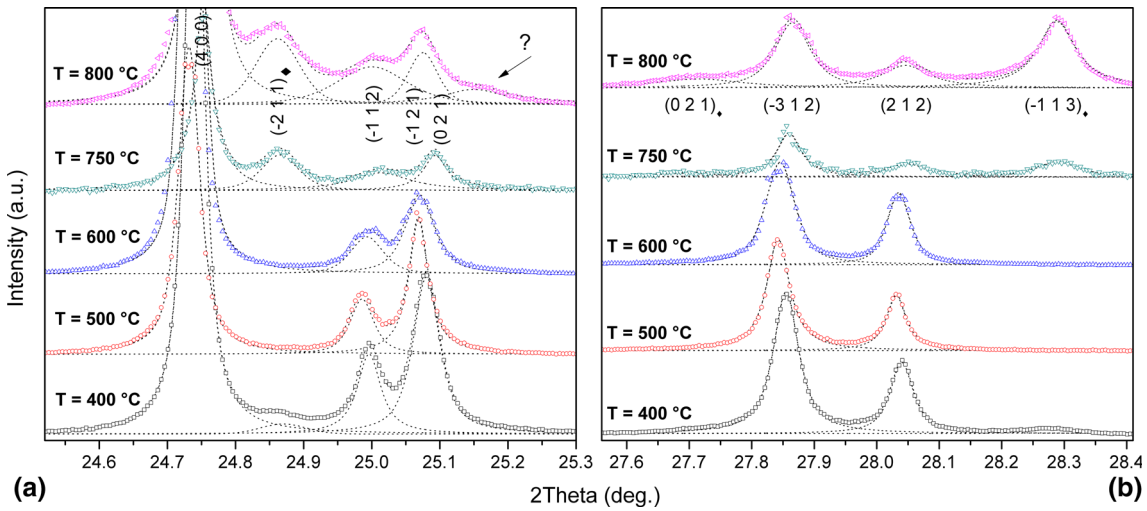

Fig. 3 Expanded views of the **a** *left* and **b** *right dotted* regions of Fig. 2 showing NLLSF to the profiles based on pseudo-Voigt functions. Temperature evolution of the involved phases is seen as well as a proper indexing of the identified phases

Table 1 Lattice parameters for the $Pb_2V_2O_7$ monoclinic phase determined for every temperature according to the NLLSF shown in Fig. 3

Temp. (°C)	a (Å)	b (Å)	c (Å)	β (deg)	$<D_C>$ (nm)
400	13.37 (0)	7.15 (5)	7.10 (4)	105.7 (1)	151.4 (7)
500	13.39 (3)	7.15 (7)	7.12 (1)	105.2 (7)	151.4 (7)
600	13.22 (7)	7.17 (6)	6.99 (9)	109.7 (2)	151.2 (3)
750	13.33 (8)	7.15 (5)	7.08 (3)	106.3 (1)	151.3 (9)
800	13.41 (6)	7.14 (9)	7.13 (7)	104.5 (9)	151.4 (9)
Ref. [3]	13.328	7.148	7.097	105.97	–
Ref. [19]	13.37	7.16	7.11	106	–
Ref. [20]	13.369	7.161	7.103	105.936	–
Ref. [21]	13.370	7.160	7.104	105.92	–

Crystallite size, $<D_C>$, was also determined and its values are also reported

start to deviate from the previous single phase ones as the orthovanadate $Pb_3(VO_4)_2$ phase stabilizes while gaining some preponderance in the recorded scans.

Even though it is out of the scope of this work, the coexistence of both phases below the critical temperature where lead losses will start to emerge, typically around 850 °C, must deserve some attention in a near future due to the ferroelectric nature of the $Pb_3(VO_4)_2$ [22, 23] that could imply the formation of a multiferroic particulate composite of practical interest. Needless to say that, for this purpose, the appropriate identification and control of the unidentified phase is still an issue that also needs to be dealt with.

According to our previous discussion, when following our proposed synthesis route, a plausible 450–700 °C temperature range could be suggested to the researcher for having the desired monophasic compound completely crystallized.

3.2 Infrared spectroscopy

As depicted in Fig. 4, the infrared vibrational spectra for 400 °C and beyond showed the typical bands for the majority phase $Pb_2V_2O_7$ [24] in all cases without evidencing the presence of the two other phases that, especially for 750 and 800 °C, are also present in our samples [25].

Given the existence of V–O–V bridges, it is possible to estimate the bridge angle (α) by considering the difference between the symmetric (ν_s) and antisymmetric (ν_{as}) stretching frequencies by means of the empirical relationship [26]:

$$\alpha = 256.41 \cdot \frac{\nu_{as} - \nu_s}{\nu_{as} + \nu_s} + 99.46 \quad (1)$$

Table 2 shows the measured stretching frequencies as well as the V–O–V bridging angles that, generally speaking, satisfy very well the theoretical conditions proposed by Wing and Callahan [27] for characterizing any M–O–M bridge angle even though slightly departing from the ideal predicted value of 122°. In our case, this difference could be associated with a

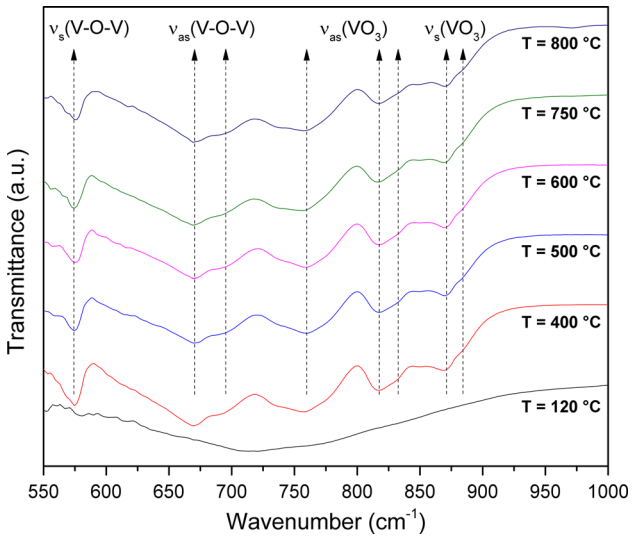

Fig. 4 Recorded FTIR spectra for the $Pb_2V_2O_7$ sol–gel-based precursors. The main stretching vibrational modes, typical for $M^{+2}(V_2O_7)^{-2}$ compounds, were detected and are highlighted in the graph

departure of the vanadium ion from its formal oxidation state +5, thus giving rise to larger interatomic distances and favoring the stabilization of the bridging structure at smaller angles [27–29]. On the other hand, the empirical nature of Eq. (1) and its determination based on datasets for mostly monocrystalline materials is another factor to take into account when explaining this discrepancy.

3.3 Xanes

X-ray absorption data were analyzed by using standard procedures: A linear background was fitted at the pre-edge region and then subtracted from the entire spectrum; the jump of the spectrum was normalized to unity with the post-edge asymptotic value by using a quadratic fit. To obtain the mean oxidation state of the metal in each sample, the energy shift of the edge relative to a Vanadium foil

Table 2 Symmetric and antisymmetric stretching frequencies determined from the measured FTIR spectra at different temperatures

Temp. (°C)	ν_s(VOV) (cm^{-1})	ν_{as}(VOV) (cm^{-1})	$\nu_{as}(VO_3)$ (cm^{-1})	$\nu_s(VO_3)$ (cm^{-1})	α (deg)
400	574.9	669.6	817.2	868.5	119.0
500	574.5	670.3	817.5	869.6	119.2
600	575.3	669.9	817.5	869.4	118.9
750	574.2	669.3	816.5	868.8	119.1
800	575.5	670.0	817.3	869.7	118.9
Ref. [26]	577	686	–	–	122

The V–O–V bridging angle (α), determined from Eq. (1), is also shown

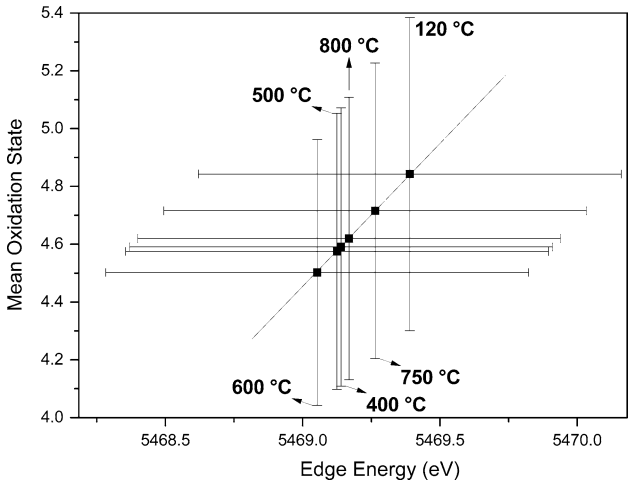

Fig. 5 Plot of mean oxidation state versus edge energy (zero of second derivative). The quantification was performed by the Wong's Method

was determined by the inflection point at the edge position of the XANES spectra—see Supplementary Information and XANES datafiles. As shown in the work of Wong et al. [30], all bound electronic transitions display a nearly linear relationship between their energy edge positions and formal oxidation state in the series of chemically similar V-compounds, e.g., oxides. This linear correlation is normally measured at the inflection point of the edge (i.e., the edge position) and in our case we take the value at the zero of second derivative. Reference compounds—in our case, metallic V (formal oxidation state 0), $VOSO_4{\cdot}nH_2O$ (formal oxidation state +4) and V_2O_5 (formal oxidation state +5)—were employed to determine a linear relationship in between the energy shift of the absorption edge vs. formal oxidation states. With this linear relationship, we can estimate the average oxidation state for V in each sample as shown in Fig. 5. Even this determination is not precise enough because the error in the energy resolution at V K-edge (see error bars in Fig. 5) is sufficient for a qualitative description of the trend of the mean oxidation state of V in V-species present in successive thermal treatments.

As can also be seen, there is some average departure from the V formal oxidation state +5 that is related to our previous discussion about the V–O–V bridging angle. In fact, except for $T = 500$ °C, there is a congruent correlation between α and the mean oxidation state that somehow supports what was said before.

3.4 Qualitative morphological description

In order to explore the morphological quality of the calcined powders, scanning electron microscopy (SEM) micrographs were recorded for powdered samples in an FEI Quanta 650 FEG microscope. Due to their relatively low quality, they have been taken out of the main body of this work but are available to the reader in the second section of the Supplementary Material. Those micrographs reveal a noticeable submicrometric granular structure that, especially for $T = 500$ °C, features some clear monoclinic facets and very regular spatial distribution and morphology.

4 Conclusions

In this work, we have studied the crystallization process of the compound $Pb_2V_2O_7$ by means of a very simple, cheap and easily adaptable sol–gel-based synthesis route that is not usually reported in literature for this compound. We have found the complete formation of the material of interest for $T = 500$ °C and, as a remark, recommended the interval 450–700 °C to maintain the appropriate crystalline quality in the final material. The final granular array showed submicrometric particles with high morphological quality.

Besides, several structural features were analyzed and discussed, specially the significant correlation between the V–O–V bridging angle and the mean oxidation state of vanadium ions in our samples.

Last but not least, the feasible coexistence of the compound with a ferroelectric phase for higher treatment temperatures, along with the remarkable morphological

quality in all cases, is something that, according to our point of view, must be thoroughly studied in future works.

Acknowledgments This work has been supported by Project No. 221541/CUValles(DECyT)/P3e-2014, Project PROINPEP-2014/CUValles and Project PROMEP-NPTC No. UDG-PTC-1080. The authors would also like to thank to CNPEM, in particular to the LNNano and LNLS staff and, most of all, to Dr. C.A. Ospina Ramírez for his kind support with SEM characterizations. Besides, the help provided by Dr. C. Velásquez-Ordoñez, CUVALLES-UdG must also be acknowledged and highly appreciated. We also thank Dr. M. Saleta from Unicamp for help on XAFS acquisition.

References

1. Blonska-Tabero A, Bosacka M (2013) Comparative studies in subsolidus areas of ternary oxide systems PbO–V_2O_5–In_2O_3 and PbO–V_2O_5–Fe_2O_3. J Therm Anal Calorim 113(1):137–145. doi:10.1007/s10973-013-2996-4
2. Bosacka M (2012) New indium lead(II) vanadate(V) in $Pb_2V_2O_7$–$InVO_4$ system and its characterization. J Alloy Compd 542:228–231. doi:10.1016/j.jallcom.2012.07.030
3. Zhou W, Tan D, Xiao W, Song M, Chen M, Xiong X, Xu J (2012) Structural properties of $PbVO_3$ perovskites under hydrostatic pressure conditions up to 10.6 GPa. J phys Condens matter Inst Phys J 24(43):435403. doi:10.1088/0953-8984/24/43/435403
4. Martin LW, Zhan Q, Suzuki Y, Ramesh R, Chi M, Browning N, Mizoguchi T, Kreisel J (2007) Growth and structure of $PbVO_3$ thin films. Appl Phys Lett 90(6):062903. doi:10.1063/1.2435944
5. Blonska-Tabero A, Filipek E (2014) New solid solution $Pb_{2-x}Sr_xFeV_3O_{11}$—Synthesis, homogeneity range and characterization. J Alloy Compd 587:148–152. doi:10.1016/j.jallcom.2013.10.144
6. Guskos N, Typek J, Zolnierkiewicz G, Szymczak R, Berczynski P, Wardal K, Blonska-Tabero A (2011) Magnetic properties of a new iron lead vanadate $Pb_2FeV_3O_{11}$. J Alloy Compd 509(32):8153–8157. doi:10.1016/j.jallcom.2011.05.114
7. Errandonea D, Popescu C, Achary SN, Tyagi AK, Bettinelli M (2014) In situ high-pressure synchrotron X-ray diffraction study of the structural stability in $NdVO_4$ and $LaVO_4$. Mater Res Bull 50:279–284. doi:10.1016/j.materresbull.2013.10.047
8. Goutaudier C, Ermeneux FS, Cohen-Adad MT, Moncorgé R, Bettinelli M, Cavalli E (1998) LHPG and flux growth of various Nd:YVO_4 single crystals: a comparative characterization. Mater Res Bull 33(10):1457–1465. doi:10.1016/s0025-5408(98)00143-3
9. Blonska-Tabero A (2010) $Pb_2Fe_2V_4O_{15}$—A new phase forming in the system $FeVO_4$–$Pb_2V_2O_7$. J Alloy Compd 508(1):42–46. doi:10.1016/j.jallcom.2010.08.028
10. Blonska-Tabero A (2009) A new iron lead vanadate $Pb_2FeV_3O_{11}$: synthesis and some properties. Mater Res Bull 44(8):1621–1625. doi:10.1016/j.materresbull.2009.04.015
11. Liu H, Hu C, Wang ZL (2006) Composite-hydroxide-mediated approach for the synthesis of nanostructures of complex functional-oxides. Nano Lett 6(7):1535–1540. doi:10.1021/nl061253e
12. Suárez-Gómez A, Saniger-Blesa JM, Calderón-Piñar F (2012) 'Universal' Synthesis of PZT (1−x)/x Submicrometric structures using highly stable colloidal dispersions: a bottom-up approach. In: Peláiz-Barranco A (ed) Advances in Ferroelectrics. InTech. doi:10.5772/51996
13. Suárez-Gómez A, Saniger-Blesa JM, Calderón-Piñar F (2010) A study on the stability of a PZT precursor solution based on the time evolution of mean particles size and pH. Mater Chem Phys 123(1):304–308. doi:10.1016/j.matchemphys.2010.04.017
14. Tolentino HCN, Ramos AY, Alves MCM, Barrea RA, Tamura E, Cezar JC, Watanabe N (2001) A 2.3 to 25 keV XAS beamline at LNLS. J Synchrotron Radiat 8(3):1040–1046. doi:10.1107/s0909049501005143
15. Suárez-Gómez A, Saniger-Blesa JM, Calderón-Piñar F (2011) A crystallization study of nanocrystalline PZT 53/47 granular arrays using a sol-gel based precursor. J Mater Sci Technol 27(6):489–496. doi:10.1016/s1005-0302(11)60096-0
16. Zyryanov VV, Lapina OB (2001) Mechanochemical synthesis and structure of new phases in the Pb–V–O system. Inorg Mater 37(3):264–270. doi:10.1023/a:1004169431601
17. Dimitrov V, Dimitriev Y (1990) Structure of glasses in PbO-V_2O_5 system. J Non-Cryst Solids 122(2):133–138. doi:10.1016/0022-3093(90)91058-y
18. Fotiev AA, Slobodin BV, Khodos MY (1988) Vanadaty: sostav, sintez, struktura, svoistva (Vanadates: Composition, Synthesis, Structure, Properties). Nauka, Moskva
19. Kawahara A (1967) La structure cristalline de la chervetite. Bulletin de la Societe Francaise de Mineralogie et de Cristallographie 90:279–284
20. Shannon RD, Calvo C (1973) Refinement of the crystal structure of synthetic chervetite, $Pb_2V_2O_7$. Can J Chem 51(1):70–76. doi:10.1139/v73-010
21. Martin K, McCarthy G (1993) ICDD Grant-in-Aid. Card 47-1735. ICDD, North Dakota State University, Fargo, USA
22. Midorikawa M, Kashida H, Sawada A, Ishibashi Y (1980) Ferroelectricity in $Pb_3(VO_4)_2$ crystal. J Phys Soc Jpn 49(3):1095–1097. doi:10.1143/jpsj.49.1095
23. Salje E, Iishi K (1977) Ferroelastic phase transitions in lead phosphate–vanadate $Pb_3(P_xV_{1-x}O_4)_2$. AcCrA 33(3):399–408. doi:10.1107/s0567739477001065
24. Baran EJ, Pedregosa JC, Aymonino PJ (1975) Das Schwingungsspektrum von $Pb_2V_2O_7$. Monatsh Chem 106(5):1085–1090. doi:10.1007/bf00906220
25. Weinstock N, Schulze H, Müller A (1973) Assignment of ν_2 (E) and ν_4 (F_2) of tetrahedral species by the calculation of the relative Raman intensities: the vibrational spectra of VO_4^{3-}, CrO_4^{2-}, MoO_4^{2-}, WO_4^{2-}, MnO_4^-, TcO_4^-, ReO_4^-, RuO_4, and OsO_4. J Chem Phys 59(9):5063. doi:10.1063/1.1680724
26. Baran EJ (1978) A correlation between the V—O—V bridge stretching frequencies and angle in divanadates. J Mol Struct 48(3):441–443. doi:10.1016/0022-2860(78)87254-8
27. Wing RM, Callahan KP (1969) Characterization of metal-oxygen bridge systems. Inorg Chem 8(4):871–874. doi:10.1021/ic50074a034
28. Brown RG, Ross SD (1972) The vibrational spectra of some condensed tetrahedral anions [X2O7]n−. Spectrochim Acta Part A 28(7):1263–1274. doi:10.1016/0584-8539(72)80096-5
29. Hezel A, Ross SD (1967) The vibrational spectra of some divalent metal pyrophosphates. Spectrochim Acta Part A 23(5):1583–1589. doi:10.1016/0584-8539(67)80381-7
30. Wong J, Messmer RP, Maylotte DH (1984) K-edge absorption spectra of selected vanadium compounds. Phys Rev B 30(10):5596–5610. doi:10.1103/PhysRevB.30.5596